Mem. S.A.It. Vol. 88, 206

Memorie della

Developments of FPGA-based digital back-ends for low frequency antenna arrays at Medicina radio telescopes

G. Naldi[1], M. Bartolini[1], A. Mattana[1], G. Pupillo[1], J. Hickish[2], G. Foster[3,4], G. Bianchi[1], A. Lingua[5], J. Monari[1], S. Montebugnoli[1], F. Perini[1], S. Rusticelli[1], M. Schiaffino[1], G. Virone[6], and K. Zarb Adami[7,8]

[1] Istituto Nazionale di Astrofisica – Istituto di Radio Astronomia di Bologna, Via Gobetti 101, I-40129 Bologna, Italy, e-mail: gnaldi@ira.inaf.it
[2] Department of Astronomy, University of California, Berkeley, CA
[3] Department of Physics and Electronics, Rhodes University, PO Box 94, Grahamstown, 6140, South Africa
[4] SKA South Africa, 3rd Floor, The Park, Park Road, Pinelands, 7405, South Africa
[5] Polytechnic of Turin, Department of Environment, Land and Infrastructure Engineering, Turin, Italy
[6] CNR, Institute of Electronics, Computer and Telecommunication Engineering, Turin, Italy,
[7] Sub-Department of Astrophysics, Department of Physics, University of Oxford, Denys Wilkinson Building, Keble Road, Oxford OX1 3RH, UK
[8] Department of Physics, University of Malta, Msida MSD 2080, Malta

Abstract. In radio astronomy Field Programmable Gate Array (FPGA) technology is largely used for the implementation of digital signal processing techniques applied to antenna arrays. This is mainly due to the good trade-off among computing resources, power consumption and cost offered by FPGA chip compared to other technologies like ASIC, GPU and CPU. In the last years several digital backend systems based on such devices have been developed at the Medicina radio astronomical station (INAF-IRA, Bologna, Italy). Instruments like FX correlator, direct imager, beamformer, multi-beam system have been successfully designed and realized on CASPER (Collaboration for Astronomy Signal Processing and Electronics Research, https://casper.berkeley.edu) processing boards. In this paper we present the gained experience in this kind of applications.

Key words. Radio astronomy – FPGA – digital signal processing – low frequency antenna arrays – correlation – beamforming – calibration – multi-beam

1. Introduction

FPGAs provide an excellent combination of flexibility and performance that makes them well-suited for moderate-scale signal processing applications such as correlators and beamformers. CASPER (Hickish et al. 2016) is an international collaboration among sev-

eral research institutes and universities whose goal is to shorten the astronomy instrument development cycle by designing modular, upgradeable hardware and a generalized, scalable architecture for combining this hardware into a signal processing instrument. Employing FPGAs, FPGA-based chip-independent signal processing libraries and packetized data routed through commercially available switches, CASPER instrument architectures look like a cluster with reconfigurable, modular computing hardware in place of CPU compute nodes. Thus, a small number of easily replaceable and upgradeable hardware modules may be connected with as many identical modules as necessary to meet the computational requirements of an application. Such an architecture can provide orders of magnitude reduction in overall cost and design time and will closely track the early adoption of state of the art IC fabrication by FPGA vendors. Also, CASPER has designed a set of open-source libraries for the Simulink/Xilinx System Generator FPGA programming language. These libraries abstract chip-specific components to provide high-level interfaces targeting a wide variety of devices. Signal processing blocks in these libraries, such as polyphase filter banks, Fast Fourier Transforms, digital down converters and vector accumulators, are parameterized to scale up and down to arbitrary sizes, and to have selectable bit widths, latencies and scaling.

We decided to adopt such solutions in order to reduce the time and cost of developing and implementing a wide range of signal processing systems for the application to low frequency antenna arrays, with FX correlators and beamformers foremost among them.

This paper begins with a presentation of the CASPER processing boards that are installed on the premises of the Medicina radio astronomical station (35 km South-East of Bologna, Italy) in 2. A digital back-end developed for the Basic Element for SKA Training II (BEST-2) array, which allows concurrent operation of an FX correlator, and a direct-imaging correlator and beamformer, is described in 3. The digital acquisition system specifically designed for an experimental array used as a test bench for antenna characterization and array calibration techniques in operative conditions is presented in 4. A multi-beaming back-end that enables space debris observations with Northern Cross radio telescope follows in 5. Final considerations are given in 6.

2. CASPER hardware at Medicina radio observatory

Since 2006 some CASPER FPGA-based processing boards have been purchased in order to fulfill the signal processing needs for several applications. We can roughly divide them in two main groups: a first and a second generation of platforms. The former are represented by the Interconnect Break-out Board (IBOB) and the Berkeley Emulation Engine (BEE2).

The IBOB features two Z-DOK connectors, to which a variety of I/O boards can be attached (including dual 1 GSa/sec ADC, quad 250 MSa/sec ADC and DAC). The IBOB has a Xilinx Virtex-II Pro XC2VP50 FPGA, and is generally used in radio astronomy applications primarily for digitizing data, performing down-conversion, filtering and FFT operations, and outputting this data over two 10GbE-compatible CX4 connectors to other boards, switches and computers. It can be used to provide a high-speed interface to BEE2 boards.

The BEE2 (Chang et al. 2005) is a general-purpose processing module based on five high-performance Xilinx FPGAs (Virtex-II Pro XC2VP70). The FPGAs are laid out in a star/ring topology with four User FPGAs in a ring and one Control FPGA connected to each user. The User FPGAs each have four independent high speed serial channels which are capable of transfering data at 10Gbps through CX4 connectors. The User FPGA ring consists of parallel connections of 138 high-speed LVCMOS traces between the FPGAs which can run at a maximum of 400Mbps. The Control FPGA has two high-speed serial channels, 64 LVCMOS traces to each User FPGA, and connections to common peripherals such as 10/100 Ethernet, USB 1.1, RS232 serial, DVI, and GPIOs. Each FPGA connects also to 4 GB of DDR2-SDRAM.

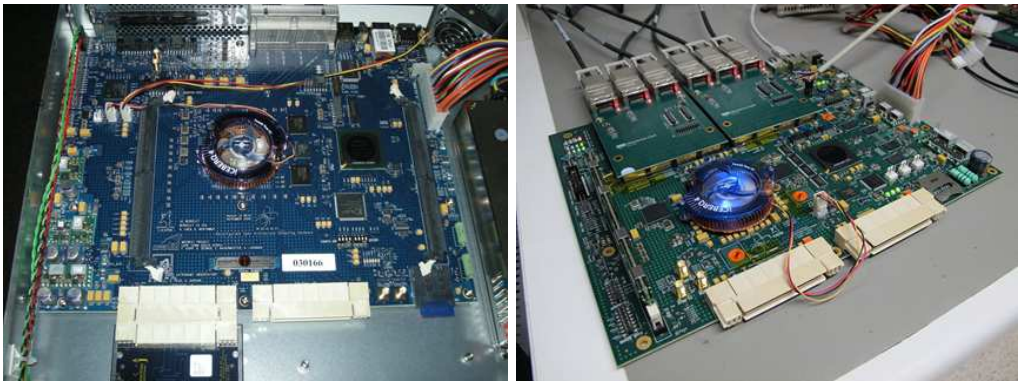

Fig. 1. ROACH1 (left) and ROACH2 (right) CASPER processing boards.

These processing boards were used to deploy a 32 inputs, 40 MHz bandwidth FX correlator operating on 8 cylinders of the Northern Cross's N/S arm in 2008. The hardware consisted of 8 IBOBs, 16 Atmel AT84AD001B dual 8-bit ADC chips (each capable of digitizing two streams at up to 1 GSa/sec) and one BEE2 (Montebugnoli et al. 2009).

ROACH1 and ROACH2 (Fig. 1) are the second generation of CASPER processing boards present at Medicina radio observatory. ROACH (Reconfigurable Open Architecture Computing Hardware) was developed thanks to a collaboration among SKA South Africa group (MeerKAT), UC Berkeley and NRAO (National Radio Astronomy Observatory) and it was intended as an upgrade to both IBOB and BEE2 merging their functionalities into a single board.

In the ROACH1 there is a single Xilinx Virtex-5 XC5VSX95T FPGA containing 94,000 logic cells and 640 multiplier/accumulators that provide 400 Gops/sec of processing power. A separate PowerPC runs Linux and is used to control the board (program the FPGA and allow interfacing between the FPGA software registers/BRAMs/FIFOs and external devices using Ethernet). Two quad data rate (QDR) SRAMs provide high-speed, medium-capacity memory (specifically for doing corner-turns), and one DDR2 DIMM provides slower-speed, high-capacity buffer memory for the FPGA. The PowerPC has an independent DDR2 DIMM in order to boot Linux/BORPH. The two Z-DOK connectors allow ADC, DAC and other interface cards to be attached to the FPGA, in the same manner as the IBOB allowed (with backwards compatibility for the ADC boards used with the IBOB). Four CX4 connectors provide a total of 40Gbits/sec bandwidth for connecting ROACH boards together, or connecting them to other XAUI/10GbE-capable devices (such as BEE2 boards, computers with 10GbE NICs and 10GbE switches).

ROACH2 was designed as the sequel to ROACH-1 using the new Xilinx Virtex-6 series of FPGAs. It maintains all the aspects that made ROACH-1 a success, but increases the overall performance in terms of processing power, IO throughput and memory bandwidth. It uses the same PowerPC 440EPx present on the ROACH-1 but adds a unified JTAG interface provided through an FTDI FT4232H IC. Other significant improvements over ROACH1 are represented by 2 Multi-gigabit transceiver break out card slots, supporting up to 8x10GbE SFP+ links or 6x10GbE CX4 links. Also ROACH2 mounts 4 x 36*2M QDR II+ SRAMs and a single 72-bit DDR3 RDIMM slot connected to the FPGA.

Besides, CASPER group developed some ADC cards with different number of inputs and sampling rates. We found of particular interest the board developed by Rick Raffanti (`https://casper.berkeley.edu/wiki/64ADCx64-12`) that is able to digitize 64 streams at up to 65 Msps. This ADC board

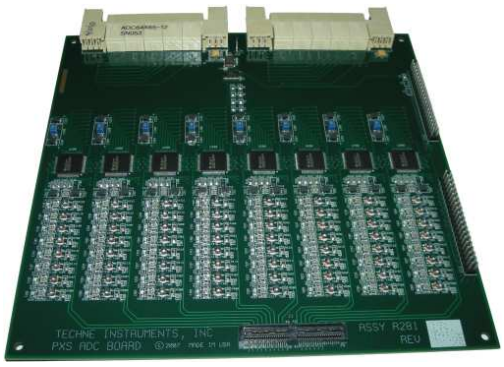

Fig. 2. The 64 input 12 bit CASPER ADC board (64ADCx64-12).

(Fig. 2) makes use of eight ADC chips, Texas Instruments ADS5272 8-channel 12-bit.

3. Implementation of a direct-imaging and FX correlator for the BEST-2 array

We present a digital back-end designed for the Basic Element for SKA Training II (BEST-2) array at the Medicina radio telescopes. This back-end is implemented on ROACH1 boards. It consists of an FX correlator and a spatial Fast Fourier Transform (FFT) processor which can be used as a direct-imaging correlator or as a beamformer, supplying high time resolution data to a pulsar and transient detection pipeline.

3.1. BEST-2 Array

BEST-2 array is a subset of the Northern Cross radio telescope, located in Medicina, and it consists of 8 East-West oriented cylindrical parabolic concentrators, each with 64 half-wave dipoles critically sampling a focal line at 408MHz. These 64 dipoles are grouped in 4 16-elements broadside sub-arrays, resulting in 4 receivers per cylinder, and a total of 32 effective receiving elements laid out on a 4-by-8 grid, depicted in Fig. 3. The cylinders, which lie on an east-west axis, can be mechanically rotated to point at a constant declination within the array pointing limits. BEST-2 was developed as a reliable, low cost analogue frontend

Table 1. The top level specifications of the BEST-2 array, a subset of the Northern Cross Radio Telescope.

BEST-2 array specifications	
Total number of receivers	32
Total collecting area	1411.2 m^2
A_{eff}/T_{sys}	11.65 m^2/K
Longest baseline (E-W)	17.04 m
Longest baseline (N-S)	70.00 m
Central frequency	408 MHz
Analogue bandwidth	16 MHz
Primary beam area	30 deg^2
North-south	5.7 deg
East-west	6.6 deg
Zenith-pointing PSF area	0.7 deg^2
North-south	31.1 arcmin
East-west	104 arcmin

to be used in SKA development, with a core design requirement of simplicity in interfacing with different digital backends (Montebugnoli et al. 2009). Extensive documentation of the development of the BEST-2 analogue chain can be found in several earlier publications (Perini 2009; Perini et al. 2009). The top level specifications of the array are shown in Table 1.

3.2. FPGA Instrumentation

The FPGA-based instrumentation for BEST-2 is made up of three interconnected ROACH1 boards. These will be referred to as the F-Engine, S-Engine and X-Engine for their respective functions. Table 2 lists the digital specifications of the implemented FPGA hardware.

The F-Engine processing node is responsible for digitization, frequency channelization and transmission of quantized antenna signals to downstream processing boards. Duplicate streams are sent from the F-Engine to the X-Engine for cross-correlation, and to the S-Engine where a spatial Fourier transform is performed. So it possible to use both the FX correlator and spatial FFT imager concurrently. This allows a streamlined process for calibrat-

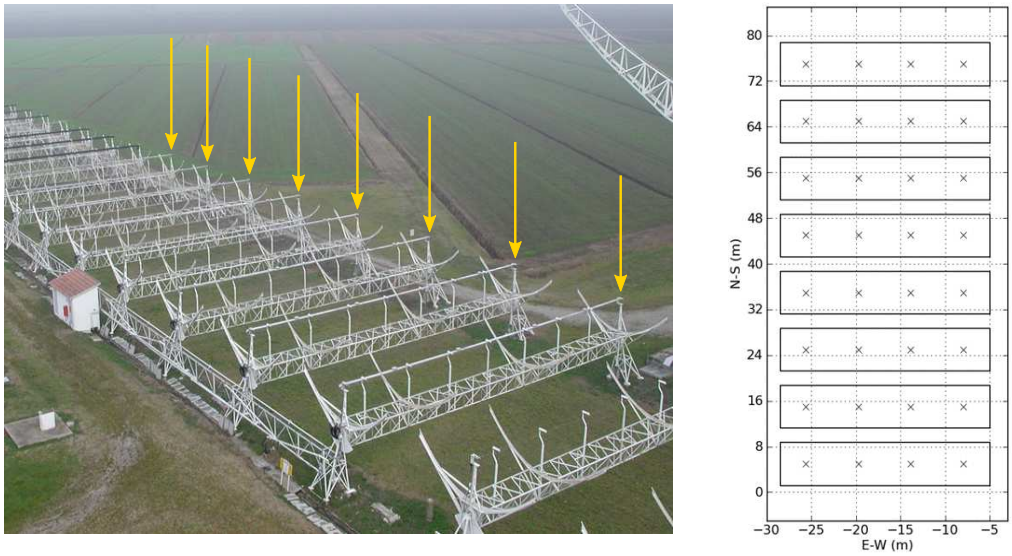

Fig. 3. The BEST-2 array is composed of eight East-West oriented cylindrical parabolic concentrators (left). The 32 effective receiving elements, indicated by crosses, lie on a regular 4x8 grid (right).

Fig. 4. The ROACH1 board, a XILINX Virtex-5 SX95T FPGA board, with the 64 input ADC connected via two Z-DOK connectors.

ing the spatial FFT imager and reduces the amount of hardware. Moreover, the simultaneous observation with both instruments permits a direct comparison between the two architectures. Signal digitization is performed using the 64ADCx64-12 ADC board. The ADC is connected via a dual Z-DOK interface (64 low-voltage differential signal pairs) to the ROACH1 board, as depicted in Fig. 4.

In this design 32 signal streams are digitized at 40 MSPS for 20 MHz of digital bandwidth, under-sampling in the second Nyquist window the IF analogue band (22-38 MHz).

The digitized band is channelized using a critically sampled 4-tap Hann filter, 2048-point polyphase filterbank (PFB) (using 18-bit coefficients) to produce 1024 complex samples per real antenna stream covering the range 398-418 MHz. Individual channel resolution is 19.53 kHz. The ROACH board is clocked at 160 MHz, four times the ADC sample rate, such that four signals are time-division multiplexed on to a single signal path. An adjustable, per channel complex gain equalizer is used for amplitude and phase corrections after channelization. In fact, the characteristics of a telescope analogue front end mean that a compensation of the instrumental bandpass must be applied to data to ensure optimal quantization of all sub-bands. During observations, an automated script samples the pre-quantized signals and statistically determines the correct equalization coefficients to achieve optimal 4-bit quantization. This script can be run at a user selected cadence during observations. The per-channel equalizers are also used to apply pre-derived amplitude and phase corrections to the signals before the 2D FFT. These values can

Table 2. Specification of the digital instrument made of the F-Engine, S-Engine and X-Engine boards which implement the direct-imaging and FX correlator architectures for BEST-2 array.

BEST-2 digital hardware specifications	
Digital bandwidth	20 MHz
ADC sampling precision	12 bit
Antenna polarizations	32 single pol.
PFB-FIR	4-tap Hann window
PFB-FFT	2048 radix-2
Freq. Channel width	19.53 kHz
Quantization	8-bit complex
X-Engine	
Auto-correlations	32
Cross-correlations	496
min $\tau_{\rm int}$	6.55 ms
Output	10 GbE (SPEAD)
S-Engine	
2D FFT	8×16
Selectable beams	128
Unique baselines	53
min $\tau_{\rm int}$	1 s
Output	1 GbE (SPEAD)
Beamformer output	10 GbE (up to 8 beams)

be dynamically set during observations to account for changes in the system calibration. After equalization the samples are re-quantized to 8-bit complex values and the data stream is duplicated and split for specific reordering for the correlator and imager. After data reordering each stream is sent over high speed XAUI at a rate of 5.12 Gbps to the X-Engine and S-Engine nodes.

The FX correlator is designed combining the F-Engine that represents the frequency channelization (as said before) and the X-Engine. The core component to the X stage is the complex multiply and accumulate (CMAC) of all pairs of independent signals for each frequency channel. A pipelined X-Engine, based on the general CASPER library (Urry et al. 2007), is used for optimal multiplier efficiency. The correlation is performed on a per-channel basis; thus, the channelized band can be split up into portions and processed in parallel across multiple X-Engines. This allows a larger bandwidth to be processed at the cost of increased logic and multiplier resource utilization. In the case of the BEST-2 system two pipelined X-Engines, each processing half of the band, are implemented in the firmware. A two-stage accumulator is used to reduce the output data rate. The first stage is fixed to give a minimum integration time to 6.55 ms; this assures that the output bandwidth to each X-Engine is approximately equal to the input bandwidth. The second accumulator, implemented using the on board QDR memory, is software controlled with integration lengths ranging from milliseconds to minutes. The array correlation matrix (ACM) is sent to a receive computer over a 10 gigabit Ethernet (10 GbE) connection. Correlation matrices are packetized as User Datagram Protocol streams using the SPEAD protocol.

In the BEST-2 back-end described here, the requirements on the direct-imaging correlator are multifold. The system should be capable of generating images of the order of second timescales, by the method described by Tegmark & Zaldarriaga (2009). Further, the system should be capable of passing formed beams at full bandwidth, i.e. without any accumulation, to downstream time-domain processing systems such as a real-time pulsar dedispersion engine (Magro et al. 2011). Instead of making individual correlations of the same baseline as in an FX correlator, the correlation of the average of each baseline can be computed. This optimization relies on the assumption that each redundant baseline measurement is indeed identical. Thus any calibration to the complex gains must be applied before the spatial FFT. Using a single frequency channel from each antenna element and the geometric array layout, a two dimensional FFT is performed to produce an image. The two-dimensional 8-by-16 FFT is performed using an 8-point parallel input FFT followed by a corner-turn and 16-point parallel input FFT. Zero-padding is added to the signals from the 4×8 antenna array before input into each stage of the transform. This yields an output of 128 complex-valued beams, from which the power is calculated and accumu-

lated. Each channel is cycled over to produce an image for each frequency band. The fourfold increase in the number of spatial transform outputs from zero-padding the inputs introduces a number of redundant calculations. In fact, the spatial transform produces 128 outputs but there are only 53 unique baselines in a 4×8 grid. Data are then accumulated in two stages. Accumulations are packetized by the ROACH's PowerPC co-processor and sent to a data recorder over 1 GbE link using the same protocol as the FX correlator. Before calculating beam powers, eight arbitrary beams can be selected and output at full data rate over 10 GbE at 16-bit precision for time domain processing.

Instrumentation was installed and tested in 2012 March for the first time. Additionally, the necessary software for general use of this instrument was developed; it is currently in regular use at the observatory. More details about the implementation and obtained results can be found in Foster et al. (2014).

4. MAD (Medicina Array Demonstrator)

Recently low frequency aperture arrays (LFAA) have gained a lot of relevance in the astronomical research field. This kind of radio telescopes and, in particular, the LFAA segment of the future Square Kilometre Array (SKA,`https://www.skatelescope.org`) will pose significant challenges in the instrumental calibration, as well as in the antenna and array characterization. To reach these tasks, an innovative technique using a customized micro Unmanned Aerial Vehicle (UAV) (hexacopter) as reference RF source has been developed (Virone et al. 2014). The UAV is equipped with an appropriate transmitting system able to radiate one or more RF tones toward the array/antenna under test. In order to test such a technique a small experimental array, the Medicina Array Demonstrator (MAD), was installed within the area of the Medicina radio astronomical station (Fig. 5).

4.1. MAD array

The MAD is composed of 9 dual-polarized Vivaldi antennas, arranged in a regular rhomboidal configuration, which are able to operate in the frequency range from 70 to more than 450 MHz. The MAD test campaigns were performed in a narrow band of 20 MHz centered around 408 MHz. This frequency was chosen in order to both exploit the existing infrastructures of the radio astronomical station and also to work in a protected band reserved to radio astronomy, avoiding possible radio frequency interferences (RFIs).

The main goal of the MAD campaigns was to validate the use of the UAV for: *(i)* the embedded element pattern measurement, *(ii)* the array beam characterization and *(iii)* the instrumental array calibration.

4.2. MAD Back-end

A digital acquisition system was specifically developed for both correlation and beamforming purposes. The firmware was designed and synthesized on ROACH1 board. As for BEST-2 back-end, signal digitization is performed using the 64ADCx64-12 ADC board. In this design only 18 signal streams (9 antennas with dual polarization) are digitized at 40 MSPS which covers the 16 MHz analogue band of the MAD system. After A/D conversion there is a polyphase filter bank (PFB) that performs the frequency channelization of the sampled data. The characteristics of the PFB are the same as BEST-2 back-end (Table 1). The PFB output is a sequence of samples, each of them belongs to a different frequency channel following a well-defined order. In this way we can pass from time domain to frequency domain. Each frequency channel has a width of 19.53 kHz and the output of the FFT stage is 36 bit complex.

The instrumental calibration in amplitude (equalization) and phase (compensation) is performed through multiplication of the signals with suitable complex gains, which are loaded in the firmware by software routines. After amplitude equalization and phase compensation stages, data are scaled and quantized down to 36 bits complex and 16 bits com-

Fig. 5. Picture of MAD array (left) and the UAV equipped with RF transmitter and dipole antenna (right).

plex respectively. This choice allows to have a good trade-off between the use of hardware resources, fitting the entire design into Virtex-5 FPGA of the ROACH board, and the correct description of the signal dynamic range.

A multiplexer is available to skip the phase equalization process depending on the mux selector signal. This is useful during the calibration procedure: in fact the first calibration step consists in correlating signals that are equalized only in amplitude (not in phase); in the second step, phase correction coefficients are loaded into FPGA thus they are applied to signals. In this last step the output of the correlator allows to check if the calibration is successfully carried out.

The beamformer system works in parallel with the correlator and its output is sent to a data storage computer via 10 GbE network and saved only when data streams from each antenna are calibrated both in amplitude and phase. Basically it calculates separately the sum of the signals of the same polarization, so we have two parallel streams at the output of the beamforming system, one for the vertical polarization and the other for the horizontal polarization. These outputs are the calibrated beams of the two polarizations.

The correlator system calculates the complex multiplications of the couples of antennas relative to a proper subset of not-redundant baselines only. Also it provides the autocorrelations of all antennas. The correlator output is sent to the data storage computer by 10 GbE network.

Similarly to calibration stage, data scaling and quantization is performed both in correlator and beamformer system before packetizing and sending output data to the storage computer. In particular data is quantized down to 32 bits complex in both cases: in this way we have a relatively low output data rate and, at the same time, the signal dynamic range is still correctly descripted. General backend specifications are summarized in Table 3.

4.3. MAD results

The MAD digital back-end was able to acquire simultaneously the signals received by all the array elements and to properly combine them in order to synthetize the array beam in the desired direction. One of the main results of MAD campaigns was that the measured embedded element patterns and array patterns were in very good agreement (within 1dB) with electromagnetic simulations (Pupillo et al. 2015) calculated by CST and FEKO software. Moreover, the back-end produced also the ACM, whose entries are the correlations of the complex voltage signals $V_i(t)$ and $V_j(t)$ of any two array elements i and j: $R_{ij}=<V_i(t)V_j^*(t)>$. A proper subset of the ACM entries has been used to calculate the phase and amplitude solutions for the instrumental calibration, taking into account the UAV position respect to each antenna.

The calibration accuracy was verified using different methods, e.g. the fringe matching technique (Fig. 7). Finally, the results of

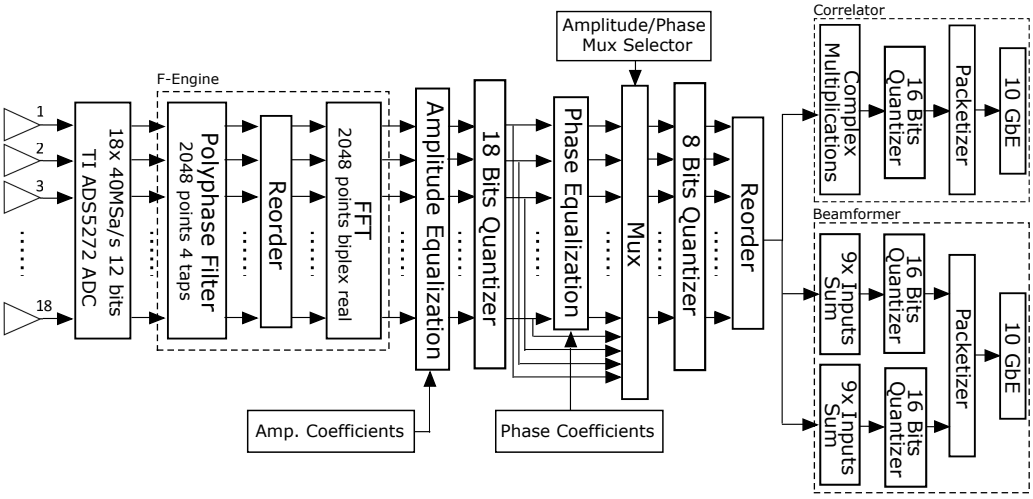

Fig. 6. Block diagram representing the firmware architecture of the correlator/beamformer systems used for MAD experiment.

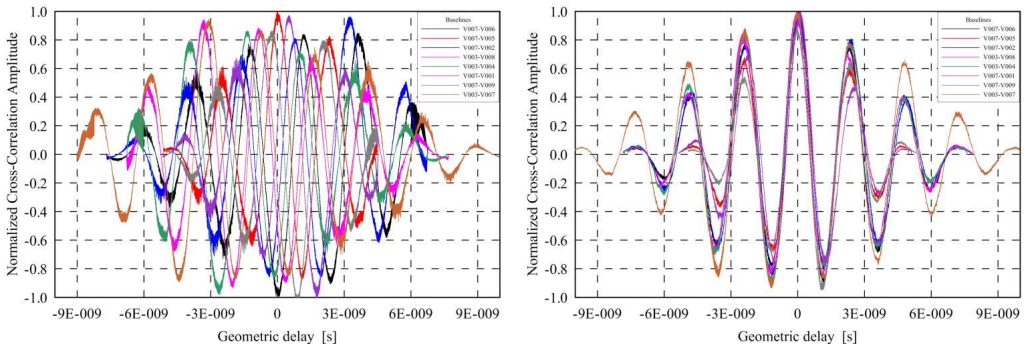

Fig. 7. Interferometric fringe patterns before (left) and after (right) the array calibration obtained with a linear UAV flight through the field of view.

a further calibration analysis, performed using statistical methods and closure quantities, confirmed the UAV system as suitable reference source for the calibration of small low-frequency arrays (Bolli et al. 2016).

5. Activity for Space Debris monitoring

Space debris are rocket bodies, tanks, pieces of broken satellites and all the rest of human activities in the Earth orbit (started on the October 4th 1957, when USSR launched the Sputnik 1 satellite). The number of these uncontrolled objects is strongly increasing: actually more than 20.000 objects larger than 10 cm are currently tracked and catalogued, but it is estimated that there are about 300 million of small objects. For this reason, the monitoring of such objects as well as the discover of new ones is becoming more and more important to avoid collisions with operative satellites or manned spacecrafts. Moreover, another big risk is represented by the uncontrolled reentry of big objects that could impact on highly populated areas.

In 2015 Italy joined a European Consortium whose mission is the space

Table 3. Main characteristics of the digital back-end designed for MAD experiment.

MAD digital back-end specifications	
Digital bandwidth	20 MHz
ADC sampling precision	12 bit
Antenna polarizations	9 dual pol.
PFB-FIR	4-tap Hann window
PFB-FFT	2048 radix-2
Freq. resolution	19.53 kHz
Time resolution	51.2 μs
Quant. after FFT	36-bit complex
Quant. after Ampl. Eq.	36-bit complex
Quant. after Phase Eq.	16-bit complex
Correlator	
Auto-correlations	18
Cross-correlations	36
Quantization	32-bit complex
Output	10 GbE
Beamformer	
Beams	2 (1 H Pol., 1 V Pol.)
Quantization	32-bit complex
Output	10 GbE

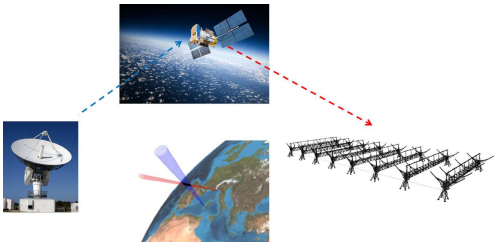

Fig. 8. Sketch that illustrates the bistatic radar architecture in which the transmitting antenna (on the left) illuminates an object and the scattered signal is received by the receiving antenna (the BEST-2, a part of the Northern Cross, on the right).

debris control. In particular, some INAF radio telescopes have been proposed as receiving part of bistatic radars.

The European Commission has recently financed, through a Grant Agreement, the Space Surveillance and Tracking (SST) program. The funds are dedicated for sensors upgrade and operating costs for observation campaigns.

5.1. Bistatic radar system

The principal technique used for monitoring Low Earth Orbit (LEO, from 200 to 2000 km of range) debris is based on radar systems operating at different frequencies and configurations. In the bistatic radar architecture the transmitting and receiving antennas are located in two different positions, typically with a distance of hundreds of kilometers between them.

The Northern Cross radio telescope, with its collecting area of about 27,000 m^2, is the largest UHF-capable antenna in the Northern hemisphere. It is composed of two perpendicular arms: the E/W (East-West) arm is a single cylindrical parabolic antenna with 564 m of length and 35 m of width; the N/S (North-South) arm is composed of 64 parallel antennas with a length of 23.5 m and a width of 7.5 m each. It is owned by the University of Bologna and operated by INAF (National Institute for Astrophysics). Using the Northern Cross as the receiving part (Fig. 8), it is possible to create a very sensitive bistatic radar system able to detect very small orbiting objects (order of tenths of square meter).

Thanks to the great number of receivers which are installed on the focal lines of this radio telescope and the large field of view (FoV, about 30 square degrees), it is possible to create many independent beams inside the FoV with proper beamforming techniques. Thus when an object transits inside the antenna FoV, beams are illuminated by the reflected (scattered) radio wave. Analysing the beam illumination sequence, the trajectory of the transiting object can be estimated with a higher level of detail with respect to a single-beam system. The data coming from the antennas is processed by a data acquisition system, which digitally assembles measured radar echoes and calculates the signal power intensity present in each beam. Also doppler shift, ranging, antenna pointing and the illumination time associated to each beam are provided by the back-end.

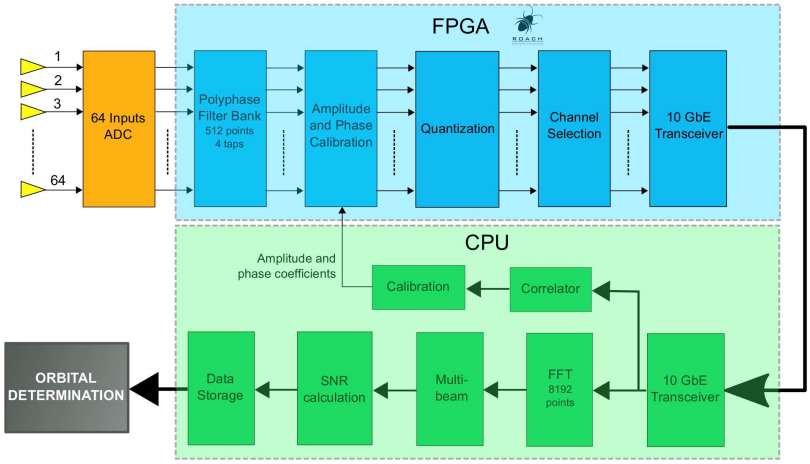

Fig. 9. Schematic representation of the two main blocks that implement the multi-beam back-end for space debris observations: the first part is designed on FPGA, the second one on CPU.

5.2. Back-end for space debris observations

The multi-beaming back-end is composed of two main parts: one designed in FPGA and the other one implemented on CPU (Fig. 9). As for BEST-2 and MAD, the digitalization is performed by the 64ADCx64-12 ADC card to convert 64 analogue signals of the N/S arm receivers in digital domain. Again the digital bandwidth is 20 MHz (sampling rate 40 MSPS). A PFB with 4-tap Hann window FIR filter and 512 points FFT is synthesized into FPGA (ROACH1 board). So the bandwidth is divided in 256 channels with 78.125 kHz of resolution each. This value ensures that any Doppler-shifted echo from a LEO target will be received within the selected band. Only the channel of interest, after a quantization stage (32 bit complex), is sent to a CPU through 10 GbE network. A second FFT is designed on the CPU to further channelize data into 8192 frequency bins (about 10 Hz of resolution), then it is realized the already mentioned multi-beam processing system that is able to create the required number of beams inside the FoV of the antenna. The data obtained by the back-end and the bistatic radar geometry (SNR associated to each synthetized beam, transit time, doppler shift, antenna pointing and ranging) are transmitted to the orbital data processing unit, which is aimed at providing an estimate of the orbital parameters of the observed object. In parallel to FFT and multi-beam blocks, the ACM is calculated in order to extract the amplitude and phase coefficients for the instrumental calibration. These coefficients are then loaded into the FPGA.

Some tests have been performed to assess the effective sensitivity and the multi-beam performance of the system. The first results are very promising: we detected objects with a RCS (Radar Cross Section) of few square meters obtaining a simulated orbit precision below 100 m (Morselli et al. 2015).

6. Conclusions

FPGA technology, thanks to the reconfigurability of these devices, allowed the use of the same DSP boards for different applications, in particular with low frequency antenna arrays. Moreover, the framework provided by CASPER group made possible the reduction of the development time of many processing systems and the easy re-use of firmware modules among several projects. So we have demonstrated that this platform is well suited for a

great number of radio astronomical applications.

At present we are working on the LFAA part of the SKA project. The first stage of DSP architecture of LFAA, i.e. coarse frequency channelization and station beamforming, is implemented in FPGA-based boards. This choice is due again to the fact that FPGAs represent a cost effective solution for the system requirements in terms of computing capacity and power consumption.

Acknowledgements. We would like to express our gratitude to Marco Poloni, Pietro Bolli, Fabio Paonessa, Irene Aicardi, Marco Piras, Paolo Maschio, Horea Bendea, Stefan Wijnholds for their fundamental contribution that allowed the success of MAD test campaigns. We would like also to thank Alessio Magro for the development of the correlation and multi-beam stage of the space debris backend. The Northern Cross Radio Telescope is a facility of the University of Bologna operated under agreement by the Institute of radio astronomy of Bologna (INAF).

References

Bolli, P. et al. 2016, Radio Sci., 51, 160

Chang, C., Wawrzynek, J., and Brodersen, R. W. 2005, IEEE Design & Test of Computers, 22, 114

Foster, G., et al. 2014, MNRAS, 439, 3180

Hickish, J. et al. 2016, Journal of Astronomical Instrumentation, 5, 1641001

Magro, A., et al. 2011, MNRAS, 417, 2642

Montebugnoli, S., et al. 2009, in Wide Field Astronomy & Technology for the Square Kilometre Array, SKADS 2009, Proceedings of Science, 63

Montebugnoli, S., et al. 2009, in Wide Field Astronomy & Technology for the Square Kilometre Array, SKADS 2009, Proceedings of Science, 58

Morselli, A., et al. 2015, A new high sensitivity radar sensor for space debris detection and accurate orbit determination, in 2nd IEEE International Workshop on Metrology for Aerospace (MetroAeroSpace) Proceedings, 562

Perini, F. 2009, in Wide Field Astronomy & Technology for the Square Kilometre Array, SKADS 2009, Proceedings of Science, 60

Perini, F., et al. 2009, in Wide Field Astronomy & Technology for the Square Kilometre Array, SKADS 2009, Proceedings of Science, 62

Pupillo, G., et al. 2015, Exp. Astron., 39, 405

Tegmark, M. and Zaldarriaga, M. 2009, Phys. Rev. D, 79, 083530

Urry, W., et al. 2007, ATA Memo 73: The ATA Correlator `http://www.seti.org/sites/default/files/ATA-memo-series/memo73.pdf`

Virone, G., et al. 2014, IEEE Antennas Wireless Propag. Lett., 13, 169